In-plane photocurrent of self-assembled $In_xGa_{1-x}As/GaAs(311)B$ quantum dot arrays

H. Z. Song, K. Akahane, S. Lan, H. Z. Xu, Y. Okada, and M. Kawabe
Institute of Applied Physics, University of Tsukuba, Tsukuba, Ibaraki 305-8573, Japan
(Received 20 November 2000; revised manuscript received 2 April 2001; published 11 July 2001)

On self-assembled $In_xGa_{1-x}As/GaAs(311)B$ quantum dots (QD's), photocurrent in the plane of QD arrays was measured under irradiation with wavelengths longer than 850 nm (1.46 eV). A sample with rather inhomogeneous QD sizes shows hopping conduction, indicating the localization of carriers in individual QD's. A two-dimensional QD superlattice, consisting of highly ordered and homogeneously sized QD's, exhibits negative differential conductance (NDC), i.e., photocurrent decrease with increasing applied voltage, in a limited electric-field range. The pre-NDC conduction is argued to arise from the miniband, which is evidenced by the photoluminescence, while the post-NDC conduction is found to be hopping as in a localized QD system, suggesting a miniband destruction under an in-plane electric field as low as $\sim 10^3\,V\,cm^{-1}$. The miniband transport is likely controlled by two-dimensional acoustic-phonon scattering.

DOI: 10.1103/PhysRevB.64.085303 PACS number(s): 73.63.Kv, 73.21.La, 72.60.+g, 72.40.+w

I. INTRODUCTION

Quantum dots (QD's) have been widely investigated for over ten years because of their potential applications in a generation of electronic and optoelectronic devices. QD-related transport has attracted special attention, as it is intimately associated with device exploration. In self-assembled quantum dots (SAQD's), most of the transport studies were devoted to the vertical motion of carriers across a single dot layer,[1–4] in which the observations arise essentially from the energy structures of isolated QD's. Carrier transfer between individual SAQD's is of more and more interest, owing to its possible application in quantum computing.[5] Two-dimensional (2D) interdot conductance was observed in InAs/GaAs (Ref. 6) and Ge/Si SAQD systems.[7–9] Due to the strong localization of QD levels, hopping conduction was identified in the plane of Ge/Si QD arrays at sufficiently low temperatures.[8,9] However, the QD wave functions can be well delocalized as the surrounding barrier becomes thin and low enough. One of its results is the strong interdot coupling through resonant tunneling, as has often been observed in multilayer-stacked SAQD's, in which the dots are vertically aligned to be 1D finite arrays.[10,11] A more interesting case is the 2D interdot coupling in the plane of the SAQD ensemble. If the periodicity of the dot array is good enough, the interdot distance is close enough, and the dot size is homogeneous enough, an infinite 2D quantum dot superlattice (QDSL) is formed with extended minibands instead of localized QD states. A 2D QDSL is attractive because it may suppress the optical-phonon scattering,[12] and can enhance the optical non-linearity.[13] The authors of Ref. 14 reported that the in-plane transport of an ordered silver QD array changes from hopping to resonant tunneling as the interdot distance is reduced. From a CdSe QD ensemble, Artemyev *et al.*[15] observed an evolution from localized to collective electronic states as the QD density increases. In an InAs/GaAs SAQD array, a large photoluminescence (PL) redshift was found to be induced by the interdot coupling through strong wave-function overlapping.[16] Recently, the optical properties of the minibands in a 2D $In_xGa_{1-x}As/GaAs$ QDSL were investigated in detail.[17,18] In this work, we compare the in-plane transport in different $In_xGa_{1-x}As/GaAs(311)B$ SAQD arrays by using photocurrent measurements. A QD ensemble with quite inhomogeneous dot sizes shows hopping transport between the localized QD states. Negative differential conductance (NDC) was observed on a 2D QDSL. This behavior is considered to result from an evolution of the transport mechanism from miniband to hopping conductions. Two-dimensional acoustic-phonon scattering is probably dominant in the miniband transport.

II. EXPERIMENTAL DETAILS

A. Sample preparation

The samples were grown by atomic-hydrogen-assisted molecular-beam epitaxy on undoped semi-insulating $GaAs(311)B$ substrates. On a 300-nm undoped GaAs buffer layer, $In_xGa_{1-x}As$ QD's were grown in the Stranski-Krastanov mode, followed immediately by a 10-nm undoped GaAs capping layer. The growth was subsequently terminated with a 30 nm $1\times10^{17}\,cm^{-3}$ Si-doped GaAs layer.

In this paper, we refer to four sample Nos. 1–4, which are different only in $In_xGa_{1-x}As$ growth. The QD growth conditions for sample Nos. 1–3 are, 8.8-ML $In_{0.4}Ga_{0.6}As$ at 460 °C, 5.5-ML $In_{0.5}Ga_{0.5}As$ at 460 °C, and 9.9-ML $In_{0.4}Ga_{0.6}As$ at 470 °C, respectively. The wetting layer thicknesses are estimated to be 5.5, 3.5, and 5.8 ML for sample Nos. 1, 2, and 3, respectively, according to the time when the reflection high-energy electron diffraction displays a transit from stringy to spotty patterns. Sample No. 4 is a control sample without any $In_xGa_{1-x}As$ growth, but with the same other layers as in sample Nos. 1–3.

B. Photocurrent measurements

On the surface of an as-grown sample, two planar contact pads, 10 μm separated from each other, were made by alloying the deposited Au:Ge (88:12) to form Ohmic contacts down to the QD layer. The voltage was applied across the gap between two electrodes, so that the current flows parallel to the sample surface. The doped top layer helps to form Ohmic contacts, but it is in fact completely depleted due to

the surface potential in the free-surface region so that the dark current is suppressed. The photocurrent was generated by irradiation with a 190-W halogen lamp normally incident onto the sample surface. A low-pass filter with cutoff at 850 nm (1.46 eV) was used in between the light source and the sample to populate the QD layer, and to constrain the simultaneous excitation in bulk GaAs matrix. The current was measured using a HP 4156B precision semiconductor parameter analyzer, with samples mounted in a table-top prober system cooled by flowing liquid He.

Detailed measurements were preformed on the samples with electrodes configuration leading to current along the $[\bar{2}33]$ direction, while other directions were checked at some points of irradiation power and temperature. Single-color irradiation was also tried as a comparison. A band-pass interference filter with a 10-nm-wide transparent window and various central wavelengths of 855–880 nm, or a monochromator, was used to replace the low-pass filter. A tunable Ti-:sapphire laser is another tool for this purpose, especially for high-intensity irradiation. Unless specially indicated, however, the data shown in this paper correspond to currents along the $[\bar{2}33]$ direction and the low-pass-filtered irradiation source.

C. Conventional measurements

As the central part of a sample, the QD's were characterized in optical properties and microstructures. The PL spectrum was measured with an excitation of the 514.5-nm line from an Ar^+ laser in a cryostat at liquid-He temperature on a sample piece cut from the same wafer as the photocurrent sample. The QD morphology was imaged on uncapped QD's, which were fabricated in nominally the same manner as the photocurrent sample: by atomic force microscopy (AFM) at room temperature in air, using a Nanoscope II system.

III. RESULTS

The representative photocurrent-voltage (I-V) curves for different samples measured at 4.5 K with an irradiation intensity of 145 mW cm^{-2}, are shown in Fig. 1. First, the photocurrent of the control sample No. 4 is much weaker than the other three samples with QD's. This indicates the validity of using the low-pass filter to ensure that the main current of a QD containing sample is in the QD layer. At high temperatures, the QD-related current is no longer much greater than the dark current and the control sample, due to the thermalized intrinsic carriers in the GaAs matrix. Accordingly, we limit our study well below 100 K in this work. It is notable that three samples with different QD's exhibit distinct I-V characteristics. Most interestingly, there is a clear NDC behavior, i.e., decreasing photocurrent with increasing voltage, in a limited range from ~1 to ~2 V in sample No. 1. The pre-NDC I-V relation is Ohmic, which is implied by a dashed line, while the post-NDC photocurrent is not Ohmic at such a low temperature. Sample No. 2 shows simple Ohmic I-V characteristics. Sample No. 3 displays something generally observed in many samples. Its behavior lies between the behaviors of sample Nos. 1 and 2. A transition between two different Ohmic conductions, both of which are guided by straight and dashed lines, occurs as the bias changes. No NDC, but a gradual decrease of differential conductance, was observed from below 1 V to above 2 V.

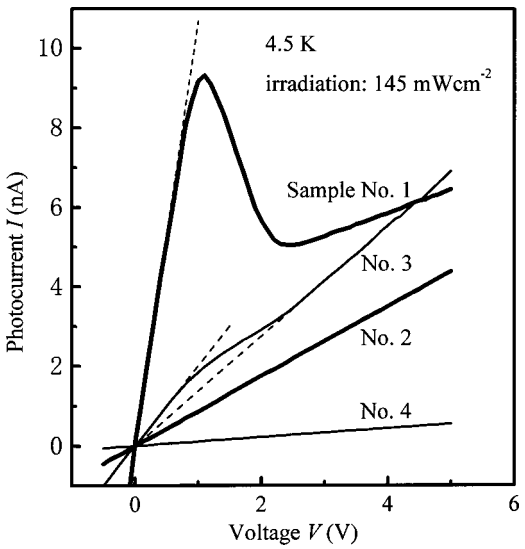

FIG. 1. In-plane photocurrent vs applied voltage measured under an irradiation intensity of 145 mW cm^{-2} at 4.5 K for different samples. The dashed lines guide the Ohmic photocurrent-voltage behaviors. Sample No. 4 is a control sample without QD's.

As a reference for understanding the sample-dependent photocurrent behavior, we examine the difference of QD's in optical and structural characteristics. Figure 2(a) illustrates the AFM images of uncapped QD's corresponding to sample Nos. 1 and 2. The QD growth condition of sample No. 1 is the same as the QDSL sample in our previous reports.[17,18] The AFM data indicate that sample No. 1 has uniform QD sizes of around 25 nm in diameter and around 1.5 nm in height, a highly ordered QD array, and a QD density of 1.4×10^{11} cm^{-2}. The QD's of sample No. 2 have rather inhomogeneous dot sizes ranging from 16 to 35 nm in diameter, and 1.5 to 3 nm in height, a disordered array, and a density of 2×10^{11} cm^{-2}. Sample No. 3 contains QD's with sizes of around 30 nm in diameter and around 2 nm in height, a density of 1.1×10^{11} cm^{-2}, but a disordered array. The QD's of all these samples are close packed, which means a negligible edge distance between neighboring dots with respect to the QD diameters. Figure 2(b) presents the PL spectra of sample Nos. 1 and 2 measured at 4.6 K under different excitation densities. The maximum excitation density is such that the photogenerated carrier density is much lower than the QD density so as to avoid state-filling effects. The narrow spectrum of sample No. 1, peaking below 1.30 eV, is redshifted, and narrowed further with decreasing excitation density. The consistency with our previous studies reveals that sample No. 1 is a 2D QDSL system, with extended miniband states.[17,18] The PL spectrum of sample No. 2, peaking at 1.34 eV, is quite broad, which is the result of a serious dot-size fluctuation. Neither a peak shift nor a shape change is observed as the excitation density changes, suggestive of an isolated QD array as conventionally fabricated. Sample No.

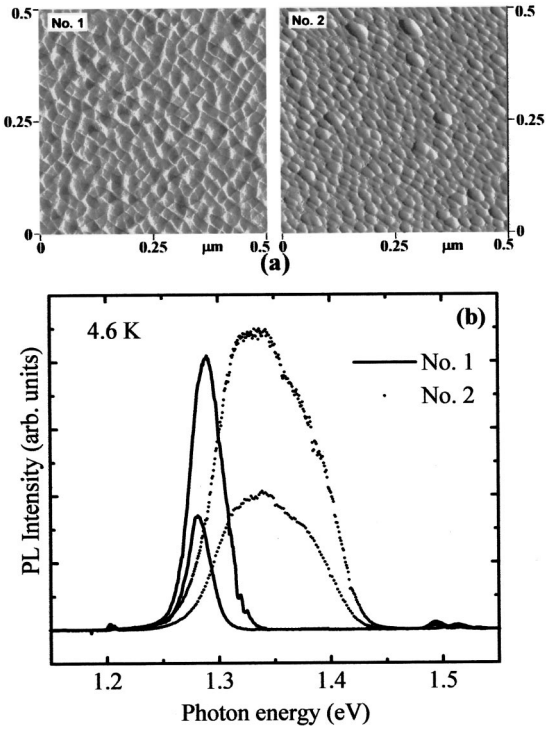

FIG. 2. (a) Atomic force microscopic images of uncapped QD's fabricated using the same growth conditions as those of sample Nos. 1 and 2. (b) The PL spectra of sample Nos. 1 and 2 measured at 4.6 K with different excitation densities.

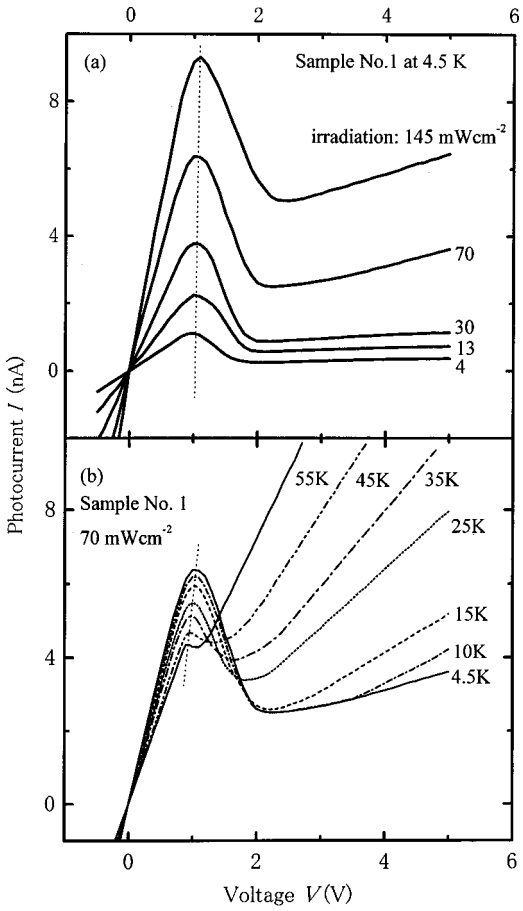

FIG. 3. The photocurrent curves of sample No. 1 (a) for different irradiation intensities at 4.5 K, (b) at different temperatures with irradiation intensity of 70 mW cm^{-2} as representative experimental results. The thin straight dotted lines indicate the irradiation and temperature dependences of the NDC onset.

3, peaking at 1.32 eV, exhibits no shift on broadness change, either. It is narrower than sample No. 2 but broader than sample No. 1.

Detailed results of photocurrent measurements are described below. We will focus on sample Nos. 1 and 2 to emphasize the specialty of NDC-related physics. A general fact is that NDC photocurrent features can be readily observed even at an irradiation intensity as low as 1 mW cm^{-2}. Figure 3(a) shows representative I-V curves of sample No. 1 under different irradiation intensities. The critical bias of NDC for sample No. 1, which corresponds to the current maximum, is almost independent of the irradiation intensity as guided by a vertical dotted line. The post-NDC photocurrent is weakly voltage dependent (non-Ohmic). As the temperature increases, its lower-bias side remains unchanged, while the higher-bias side arises to become Ohmic. A completely Ohmic post-NDC conduction appears above a certain temperature, which decreases slightly from 20 to 10 K as the irradiation is enhanced. This is visible in Fig. 3(b), where we show a series of I-V curves measured at different temperatures, with an irradiation intensity of 70 mW cm^{-2}. In contrast to the varying character of post-NDC photocurrent, there is always an Ohmic pre-NDC photocurrent in the present measurement range. What is more important, one can see opposite temperature dependences of the pre-and post-NDC photocurrents. The pre-NDC photocurrent decreases, while the post-NDC photocurrent increases with increasing temperature. As shown by the short dotted line in Fig. 3(b), the NDC onset voltage decreases slightly as the temperature rises. Furthermore, the NDC feature of sample No. 1 becomes weaker and weaker as the temperature is raised, and is no longer accessible above 60 K. As for sample No. 2, the simple Ohmic I-V relation remains for any irradiation intensity and temperature measured by us.

Corresponding to an Ohmic photocurrent, there is a well-defined conductance $G=I/V$. Shown in Fig. 4, by scattered symbols, are the irradiation-intensity (p) dependences of the conductance. The dashed lines, which are proportional fittings of measured data, show that the conductance of sample No. 2 and the post-NDC conductance of sample No. 1 are proportional to the irradiation power. Although only an example is shown (20 K for sample No. 1 and 4.5 K for sample No. 2), this behavior is general over all the temperatures available for these two Ohmic conductions. Nevertheless, the pre-NDC conductance of sample No. 1 depends sublinearly on the irradiation intensity at any temperature, as shown by the scattered solid symbols in Fig. 4. Figure 5 illustrates the temperature (T) dependences of the conductance of sample Nos. 1 and 2 by scattered symbols. The pre-NDC conductance of sample No. 1 is nearly constant at low temperatures, but obviously decreases at higher temperatures. The post-NDC conductance of sample No. 1 and the conductance of

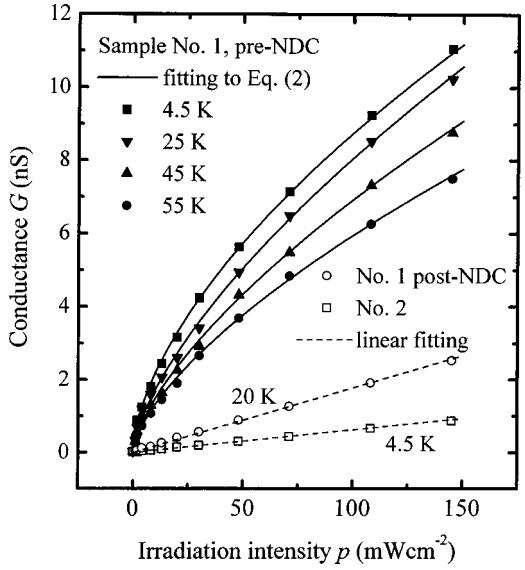

FIG. 4. Scattered symbols: the measured irradiation-intensity dependence of the pre-NDC conductance of sample No. 1 at different temperatures, that of the post-NDC conductance of sample No. 1 at 20 K and that of the conductance of sample No. 2 at 4.5 K. Solid lines: curves fitted by Eq. (2), in which the parameter α is 0.37, 0.34, 0.33, and 0.35 at 4.5, 25, 45, and 55 K, respectively; Dashed lines: indication of proportional irradiation dependence of the conductance.

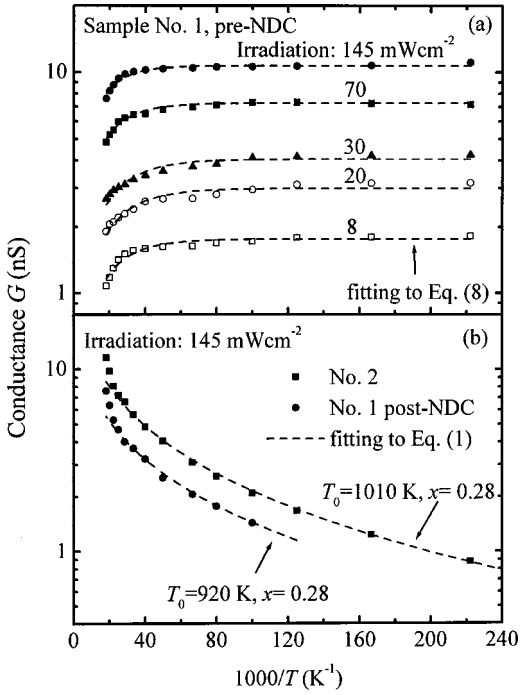

FIG. 5. Scattered symbols: the measured temperature dependence of (a) the pre-NDC conductance of sample No. 1 under different irradiation intensities, and (b) the post-NDC conductance of sample No. 1 and the conductance of sample No. 2 with an irradiation intensity of 145 mW cm^{-2}. Dashed lines: (a) curves fitted according to Eq. (8), with parameter $\bar{E}_{\mathrm{ph}}$ (average acoustic-phonon energy) being equal to 5.1, 4.5, 4.6, 5.6, and 6.6 meV from the bottom to the top curves. (b) Curves fitted by Eq. (1) for the measured data below 40 K.

sample No. 2 are thermally activated, but is not simple exponential function of $1/T$.

The above data are those corresponding to current along the $[\bar{2}33]$ direction, and the low-pass filtered irradiation. Considering the possible anisotropy on the GaAs (311) surface, such as the 1D corrugation structure along the $[\bar{2}33]$ direction reported previously,[19,20] we compared the photocurrent along the $[01\bar{1}]$ direction and two diagonal directions with respect to $[\bar{2}33]$ and $[01\bar{1}]$. Under our experimental condition, the current difference between these directions is less than 10%, which we can not exclusively ascribe to the microstructural anisotropy of the GaAs (311)B surface. This is probably because the roughness or fluctuation due to the QD distribution, which shows no meaningful anisotropy in our present samples, is larger than that due to the atomically scaled 1D corrugation structure on the (311) surface.[19,20] In addition, the photocurrent in the case of single-color irradiation shows no NDC behavior until the irradiation intensity is higher than 60 mW cm^{-2}. The observable NDC feature is much weaker than that for low-pass-filtered irradiation with the same intensity.

IV. DISCUSSION

A. Hopping conduction

Here we begin by discussing the result of sample No. 2, as is relatively simple. Detailed examinations demonstrate that the conductance of sample No. 2 follows a stretched exponential equation

$$G = G_0 e^{-(T_0/T)^x}, \tag{1}$$

where G_0, T_0, and x are constants. This is characteristic of the variable-range hopping of localized carriers, which was widely studied in amorphous semiconductors and other systems.[21] A conventional SAQD array, as a typical localized-state system, is expected to show hopping transport, which has been proved in self-assembled Ge/Si QD's.[8,9] The post-NDC conductance of sample No. 1 follows Eq. (1) as well. As indicated by the dashed lines in Fig. 5(b), the fittings of the data below 40 K to Eq. (1) give a power factor $x = 0.28 \pm 0.04$, which is universal over all the irradiation intensities for both samples. It is close to the theoretical value of 1/3 for a 2D hopping conductivity.[8,9,22] The data above 40 K follow Eq. (1), with x being close to 0.5 (not shown), which is consistent with the observation in Ge/Si SAQD.[9] The characteristic temperature T_0 in Eq. (1) is determined by the density of localized states and the localization length.[8,9,21] In Ge/Si QD's, T_0 can vary from 400 to 1200 K. Our fitted values, 920 ± 40 K for sample No. 1 and 1010 ± 50 K for sample No. 2, are thus reasonable for the hopping explanation.

The irradiation dependence of hopping conductance in Fig. 4 looks different from the peak behavior of the hopping current versus the carrier density observed in Ge/Si QD's, in which the maximum occurs when the conducting energy

level is half-filled, as this maximizes the product of possible initial and final states in hopping process.[8] As a matter of fact, the photocarrier density in our case is far below the half-filling of the ground states of QD's, which keeps the final states of hopping processes almost always empty. This accounts for the proportional hopping conductance versus the irradiation intensity. The above analysis indicates that the highly biased sample No. 1 is an isolated SAQD system in which QD states are localized in individual dots, as in sample No. 2.

B. NDC mechanism

As mentioned in Sec. III, the optical properties signify the miniband formation in the 2D QDSL sample No. 1.[17,18] The temperature dependence of the pre-NDC conductance is consistent with bandlike transport in 1D superlattices.[23] Then the localization of QD states in sample No. 1, under an electric field, is a result of miniband destruction. This is similar to the well-known Stark localization or electric-field-induced electron localization in 1D semiconductor superlattices.[23,24] High mobility is expected from miniband transport under a weak electric field, while the mobility drops remarkably under a strong electric field, since the hopping process has a low probability.[25] In other words, the observed NDC of sample No. 1 is the result of a change of the transport mechanism from miniband conduction to hopping between localized QD states.

As a necessary condition, the miniband width should be larger than the inhomogeneous broadening for both a 1D superlattice and a 2D QDSL. According to the Stark localization in 1D superlattices, the onset of NDC corresponds to the destruction of the miniband, which occurs at an electric field F_c, such that the average potential drop across superlattice period d is equal to the miniband width Δ, i.e., $F_c = \Delta/ed$, where e is the electronic charge. Simply from this criterion, the estimated miniband width of our QDSL is less than 5 meV, which is much smaller than the inhomogeneous broadening of a couple of tens of meV. To understand this ambiguity, we think that, due to the 2D characteristics of QDSL and the 1D electric field, the condition for 2D QDSL destruction is not as simple as that for 1D superlattices. Additionally, it was found that Be doping in the capping layer, even as slight as $\sim 10^{15}\,\mathrm{cm}^{-3}$, can destroy the miniband.[26] It is suggested that the QDSL miniband is not robust against some disturbance, which herein is an in-plane electric field as low as $\sim 10^{3}\,\mathrm{V\,cm}^{-1}$. Since the electric field dominates when changing the miniband, the critical field of the NDC is almost independent of the irradiation power, well below the limit of effective exciton-exciton interaction for degrading the miniband coherence.[17] The weak temperature dependence of the critical field of the NDC suggests that the thermalization of carriers makes a small contribution in destroying the miniband at temperatures below 60 K.

C. Miniband transport

To study the miniband transport, we first analyze the irradiation dependence of the pre-NDC photocurrent of sample No. 1. We find that the sublinear dependence of the pre-NDC conductance on the irradiation intensity can be well fitted by a power law

$$G \propto p^{1-\alpha}, \tag{2}$$

with $\alpha = 0.35 \pm 0.02$, as shown by the solid lines in Fig. 4. To settle the microscopic mechanism, we need to associate the irradiation power with a conductive photocarrier concentration. This is complicated in principle, because, in contrast to the good periodicity in 1D semiconductor superlattices, there are large dots in our QDSL which result in localized states below the miniband mobility edge.[17,18] The photocarriers absorbed by the miniband can thus be trapped into large dots, which will lead to a reduction of conductive carriers. However, this trapping is effectively reduced by direct photoabsorption in the large dots, because the low-pass filter extends the irradiation spectrum down below the mobility gap. This is proved by the fact that NDC is almost unobservable or rather weak if a single-color resonant irradiation source is used. Although the detailed mechanism is not clear yet, we may use this fact to suppose that the miniband carrier density n is proportional to the irradiation intensity p. Accordingly, we have the miniband mobility

$$\mu \propto G/n \propto n^{-\alpha}, \tag{3}$$

in which G follows Eq. (2). This relation, together with the fitted power factor $\alpha \approx 0.35$, is surprisingly identical within experimental error to a well-explained observation in the inversion layer of Si/SiO_2 interface: $\mu \propto n^{-1/3}$ in the case of a negligible impurity density with respect to the carriers.[27] The explanation in Ref. 27 is the scattering by acoustic phonons on the Si surface. In the present QDSL, undoped QD's and the 10-nm undoped capping layer match the requirement of few impurities. Consequently, the miniband transport in the 2D QDSL is probably controlled by the scattering of some 2D phonons in the $In_{0.4}Ga_{0.6}As/GaAs$ QD layer.

We shall now examine the validity of phonon scattering by studying the temperature dependence of the pre-NDC conductance. Theoretically, the first-order phonon-scattering rate can be given simply by the golden rule[28]

$$\frac{1}{\tau_{\mathrm{if}}} = \frac{2\pi}{\hbar} \sum_{\mathbf{q}} |M_{\mathbf{q}}^{\mathrm{if}}|^2 \left(\frac{1}{e^{E_{\mathrm{ph}}(\mathbf{q})/kT} - 1} + 1 \right) \delta[E_0 - E_{\mathrm{ph}}(\mathbf{q})], \tag{4}$$

where E_0 is the energy difference from the initial (i) to the final (f) states, k is the Boltzmann constant, $\mathbf{q}$ is the wave vector of the phonon, E_{ph} is the energy of the phonon, and the scattering matrix element

$$M_{\mathbf{q}}^{\mathrm{if}} = \alpha_q \langle i | e^{i\mathbf{q}\cdot\mathbf{r}} | f \rangle, \tag{5}$$

where $\mathbf{r}$ is a position vector, q is the length of $\mathbf{q}$, and

$$\alpha_q \propto \begin{cases} q^{1/2} & \text{(acoustic phonon)} \\ q^{-1} & \text{(optical phonon).} \end{cases} \tag{6}$$

As an approximation, we introduce $M_{\mathbf{q}}$ to present the total contribution of all possible $|i\rangle$ and $|f\rangle$ states. In the mean-

time, we convert the summation over **q** into an integral. Then we have the overall scattering rate for one branch of phonons:

$$\frac{1}{\tau} \propto \int d\mathbf{q} |M_{\mathbf{q}}|^2 / (1 - e^{-E_{\mathrm{ph}}(\mathbf{q})/kT}). \tag{7}$$

Here we assume a negligible temperature dependence of $M_{\mathbf{q}}$; then the temperature dependence of τ is mainly determined by the factor $1-\exp(-E_{\mathrm{ph}}/kT)$, but will somehow be influenced by $M_{\mathbf{q}}$. According to the result of phonon scattering in QD's, $M_{\mathbf{q}}$ is governed by α_q when q is small, while it rapidly decays to zero when q is large.[28] Owing to a lack of knowledge about miniband wave functions, it is difficult to obtain the exact $M_{\mathbf{q}}$. By mathematical examinations of various forms of $M_{\mathbf{q}}$, we learned that the calculated result from Eq. (7) can be well modeled by

$$\tau \propto 1 - e^{-\overline{E}_{\mathrm{ph}}/kT}, \tag{8}$$

where $\overline{E}_{\mathrm{ph}}$ is a somewhat average value of the phonon energy. One exception is the case of an acoustic phonon with a rapid decay of $M_{\mathbf{q}}$ from $q=0$, which seldom happens due to a power-law increase of α_q in Eq. (6).

Fitting the temperature dependence of the pre-NDC conductance of sample No. 1 to Eq. (8), as $G \propto \mu \propto \tau$, we find a good match between theory and experiment, as shown by the dashed lines in Fig. 5(a). At the same time, the fittings yield average phonon energies of 4.5–6.6 meV. Such small values are hardly compatible with optical phonons, whose energies in bulk GaAs and InAs are higher than 24 meV.[29] In addition, as in bulk semiconductors, the optical phonon scattering may disappear much faster at low temperatures than acoustic phonons.[30] On the other hand, Raman scattering of acoustic phonons in SAQD's has been readily observed.[31,32] It was shown that acoustic-phonon modes in a 1D Ge/Si QDSL are substantially enhanced with respect to the material without QD's.[32] Especially at low temperatures, acoustic-phonon scattering was found to be the dominant mechanism of carrier relaxation in QD's.[33] Accordingly, acoustic-phonon scattering is more likely than optical-phonon scattering to be the dominating mechanism. The 2D character of acoustic phonons here may originate from the strain field in the plane of the 2D QDSL.

Equation (8) can be reduced to the simple relation $\mu \propto T^{-1}$ seen in Ref. 23 at sufficiently high temperatures. This implies the self-consistency of our above argument of 2D acoustic-phonon scattering in the miniband transport.

D. Resonant tunneling

What has not been discussed so far is the non-Ohmic post-NDC conduction of sample No. 1 at low temperatures. As a possible interpretation, we ascribe this to the resonant tunneling between neighboring dots, which occurs easily because of the better dot-size homogeneity than in sample No. 2. Since the hopping (phonon-assisted tunneling) is thermally activated, it will exceed the resonant tunneling at higher temperatures, as shown in Fig. 3(b). The unchanged part of the post-NDC photocurrent of sample No. 1 at low temperatures is in agreement with the weak temperature dependence of the resonant tunneling.[9]

V. CONCLUSION

In summary, we studied the in-plane photocurrent of different self-assembled $In_xGa_{1-x}As$ QD arrays under weak irradiation, with photon energies lower than the band gap of the GaAs matrix. Hopping transport was observed in a QD array with severely fluctuating dot sizes, indicating the localization of carriers in individual QDs. The 2D QDSL exhibits a clear NDC behavior in a limited electric-field range. The pre-NDC conduction is ascribed to miniband transport, which is probably dominated by 2D acoustic-phonon scattering. The same hopping conduction as that in isolated SAQD's was observed after NDC, suggesting that the extended miniband is destroyed by an electric field as low as $\sim 10^3$ V cm^{-1}.

ACKNOWLEDGMENTS

We would like to thank the Cryogenic Center of the University of Tsukuba for assistance in PL measurements. This work was supported by a Grant-in-Aid for Scientific Research on the Priority Area ''Single Electron Devices and Their High-Density Integration'' from the Ministry of Education, Science, Sports and Culture, by the project of ''Analysis and Control of the Self-Organization Mechanism of Substances and Materials'' from the Science and Technology Agency, and by the program ''Research for the Future'' from the Japan Society for the Promotion of Science.

[1] I. E. Itskevich, T. Ihn, A. Thornton, M. Henini, T. J. Foster, P. Moriarty, A. Nogaret, P. H. Beton, L. Eaves, and P. C. Main, Phys. Rev. B **54**, 16 401 (1996).

[2] M. Narihiro, G. Yusa, Y. Nakamura, T. Noda, and H. Sakaki, Appl. Phys. Lett. **70**, 105 (1997).

[3] R. J. Luyken, A. Lorke, A. O. Govorov, J. P. Kotthaus, G. Medeiros-Ribeiro, and P. M. Petroff, Appl. Phys. Lett. **74**, 2486 (1999).

[4] L. Chu, M. Arzberger, A. Zrenner, G. Böhm, and G. Abstreiter, Appl. Phys. Lett. **75**, 2247 (1999).

[5] M. S. Sherwin, A. Imamoglu, and T. Montroy, Phys. Rev. A **60**, 3508 (1999).

[6] V. A. Kul'bachinskiĭ, V. G. Kytin, R. A. Lunin, A. V. Golikov, I. G. Malkina, B. N. Zvonkov, and Yu. N. Saf'yanov, Fiz. Tekh. Poluprovodn. **33**, 316 (1999) [Semiconductors **33**, 318 (1999)].

[7] A. I. Yakimov, C. J. Adkins, R. Boucher, A. V. Dvurechenskii, A. I. Nikiforov, O. P. Pchelyakov, and G. Biskupski, Phys. Rev. B **59**, 12 598 (1999).

[8] A. I. Yakimov, A. V. Dvurechenskii, V. V. Kirienko, and C. J. Adkins, J. Phys.: Condens. Matter **11**, 9715 (1999).

[9] A. I. Yakimov, A. V. Dvurechenskii, A. I. Nikiforov, and C. J. Adkins, Phys. Status Solidi B **218**, 99 (2000).
[10] G. S. Solomon, J. A. Trezza, A. F. Marshall, and J. S. Harris, Jr., Phys. Rev. Lett. **76**, 952 (1996).
[11] R. Provoost, M. Hayne, V. V. Moshchalkov, M. K. Zundel, and K. Eberl, Appl. Phys. Lett. **75**, 799 (1999).
[12] H. Sakaki, Solid State Commun. **92**, 119 (1994).
[13] T. Takagahara, Surf. Sci. **267**, 310 (1992).
[14] G. Markovich, C. P. Collier, and J. R. Heath, Phys. Rev. Lett. **80**, 3807 (1998).
[15] M. V. Artemyev, A. I. Bibik, L. I. Gurinovich, S. V. Gaponenko, and U. Woggon, Phys. Rev. B **60**, 1504 (1999).
[16] M. V. Maximov, A. F. Tsatsul'nikov, B. V. Volovik, D. A. Bedarev, A. Yu. Egorov, A. E. Zhukov, A. R. Kovsh, N. A. Bert, V. M. Ustinov, P. S. Hop'ev, Zh. I. Alferov, N. N. Ledentsov, D. Bimberg, I. P. Soshnikov, and P. Werner, Appl. Phys. Lett. **75**, 2347 (1999).
[17] S. Lan, K. Akahane, H. Z. Song, Y. Okada, M. Kawabe, T. Nishimura, and O. Wada, Phys. Rev. B **61**, 16 847 (2000).
[18] S. Lan, K. Akahane, H. Z. Song, S. Nishikawa, Y. Okada, O. Wada, and M. Kawabe, J. Appl. Phys. **88**, 227 (2000).
[19] L. Geelhaar, J. Máquez, and K. Jacobi, Phys. Rev. B **60**, 15 890 (1999).
[20] Z. M. Wang, L. Däweritz, and K. H. Ploog, Appl. Phys. Lett. **78**, 712 (2001).
[21] H. Iwano, S. Zaima, T. Kimura, K. Matsuo, and Y. Yasuda, Jpn. J. Appl. Phys., Part 1 **33**, 7190 (1994).
[22] T. Ando, A. B. Fowler, and F. Stern, Rev. Mod. Phys. **54**, 445 (1982).
[23] F. Capasso, K. Mohammed, and A. Y. Cho, IEEE J. Quantum Electron. **QE-22**, 1853 (1986).
[24] A. Sibille, J. F. Palmier, F. Mollot, H. Wang, and J. C. Esnault, Phys. Rev. B **39**, 6272 (1989).
[25] A. Ya. Shik, Fiz. Tekh. Poluprovodn. **8**, 1841 (1974) [Sov. Phys. Semicond. **8**, 1195 (1975)].
[26] S. Lan, K. Akahane, K.-Y. Jang, T. Kawamura, Y. Okada, M. Kawabe, T. Nishimura, and O. Wada, Jpn. J. Appl. Phys., Part 1 **38**, 2934 (1999).
[27] H. Ezawa, S. Kawaji, T. Kuroda, and K. Nakamura, Surf. Sci. **24**, 659 (1971).
[28] T. Inoshita and H. Sakaki, Phys. Rev. B **46**, 7260 (1992).
[29] *Physics of Group IV Elements and III-V Compounds*, edited by O. Madelung, Landolt-Börnstein, New Series, Group III, Vol. 17, Pt. a (Springer-Verlag, 1982).
[30] J. M. Ziman, *Electrons and Phonons* (Oxford University Press, Oxford, 1972), p. 438.
[31] J. P. Huntzinger, J. Groenen, M. Cazayous, A. Mlayah, N. Bertru, C. Paranthoen, O. Dehaese, H. Carrère, E. Bedel, and G. Armelles, Phys. Rev. B **61**, R10 547 (2000).
[32] J. L. Liu, G. Jin, Y. S. Tang, Y. H. Luo, K. L. Wang, and D. P. Yu, Appl. Phys. Lett. **76**, 586 (2000).
[33] P. Hawker, A. J. Kent, and M. Henini, Appl. Phys. Lett. **75**, 3832 (1999).